AFGL-TR-76-0119
ENVIRONMENTAL RESEARCH PAPERS, NO. 564

ATS-6 40- and 360-MHz Differential Phase Measurements

FREDERICK F. SLACK

2 June 1976

IONOSPHERIC PHYSICS DIVISION PROJECT 4643
AIR FORCE GEOPHYSICS LABORATORY
HANSCOM AFB, MASSACHUSETTS 01731

AIR FORCE SYSTEMS COMMAND, USAF

This technical report has been reviewed and is approved for publication.

FOR THE COMMANDER:

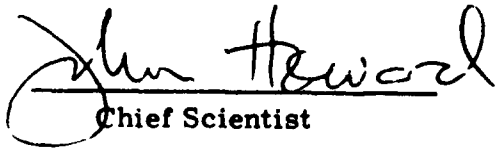

Chief Scientist

Qualified requestors may obtain additional copies from the Defense Documentation Center. All others should apply to the National Technical Information Service.

Unclassified

SECURITY CLASSIFICATION OF THIS PAGE (When Data Entered)

REPORT DOCUMENTATION PAGE

READ INSTRUCTIONS BEFORE COMPLETING FORM

1. REPORT NUMBER: AFGL-TR-76-0119
2. GOVT ACCESSION NO.:
3. RECIPIENT'S CATALOG NUMBER:

4. TITLE (and Subtitle): ATS-6 40- AND 360-MHz DIFFERENTIAL PHASE MEASUREMENTS

5. TYPE OF REPORT & PERIOD COVERED: Scientific. Interim.

6. PERFORMING ORG. REPORT NUMBER: ERP No. 564

7. AUTHOR(s): Frederick F. Slack

8. CONTRACT OR GRANT NUMBER(s):

9. PERFORMING ORGANIZATION NAME AND ADDRESS:
Air Force Geophysical Laboratory/LIR
Hanscom AFB
Massachusetts 01731

10. PROGRAM ELEMENT, PROJECT, TASK AREA & WORK UNIT NUMBERS:
62101F
46430103

11. CONTROLLING OFFICE NAME AND ADDRESS:
Air Force Geophysical Laboratory/LIR
Hanscom AFB
Massachusetts 01731

12. REPORT DATE: 2 June 1976

13. NUMBER OF PAGES: 30

14. MONITORING AGENCY NAME & ADDRESS (if different from Controlling Office):

15. SECURITY CLASS. (of this report): Unclassified

15a. DECLASSIFICATION DOWNGRADING SCHEDULE:

16. DISTRIBUTION STATEMENT (of this Report)

Approved for public release; distribution unlimited.

17. DISTRIBUTION STATEMENT (of the abstract entered in Block 20, if different from Report)

18. SUPPLEMENTARY NOTES

Presented at COSPAR Meeting 1-4 June 1976

19. KEY WORDS (Continue on reverse side if necessary and identify by block number)

Ionospheric propagation	Traveling ionospheric disturbance
Ionospheric scintillation	Total electron content
Phase scintillation	Ionospheric refraction
RF phase measurement	Electron density

20. ABSTRACT (Continue on reverse side if necessary and identify by block number)

Equipment employing new cross-correlation design concepts for receiving and processing weak rf signals in a noisy environment is described. It is shown how this equipment becomes an integral part of the instrumentation for measuring the differential phase between the ATS-6 satellite 40- and 360-MHz coherent cw signals that have been propagated through the ionosphere.

DD FORM 1 JAN 73 1473 EDITION OF 1 NOV 65 IS OBSOLETE

Unclassified

SECURITY CLASSIFICATION OF THIS PAGE (When Data Entered)

Unclassified

SECURITY CLASSIFICATION OF THIS PAGE(When Data Entered)

The relationship between 40-MHz phase and amplitude scintillation was developed using differential phase data from the ATS-6 geostationary satellite. The 40- and 360-MHz coherent signals were propagated through the ionosphere and received on the 150-ft radio telescope at the Sagamore Hill Radio Observatory.

The analysis of the computerized data was based on 13 consecutive days of active scintillation in November 1974. It shows that amplitude and phase scintillation occurred simultaneously only 53 percent of the time, indicating that application of the equivalent thin diffracting screen theory is invalid for describing the data for the remaining 47 percent of the time. Statistical comparisons suggest that daytime amplitude scintillations were apparently caused by ionospheric focusing mechanisms since phase scintillation proved to be almost exclusively a nighttime phenomena.

The differential phase data from the same source is analyzed in a manner that reveals many of the ionospheric interactions that affect space communications. The interactions are further reduced into the following parameters that describe ionospheric conditions that relate to rf propagation:

1. Total electron content (TEC)
2. Changes in electron density, assuming height
3. Equivalent slab thickness, assuming height
4. A continuous measurement of phase velocity
5. A continuous measurement of rate of change of TEC
6. A continuous measurement of rate of change of refractive index
7. A continuous measurement of angle of arrival.

The influence that the traveling ionospheric disturbances (TID) have on the phase of the 40-MHz signal receives special emphasis, and it is shown how the presence of TID aids in the analysis.

Unclassified

SECURITY CLASSIFICATION OF THIS PAGE(When Data Entered)

Contents

Illustrations

Illustrations

ATS-6 40- and 360-MHz Differential Phase Measurements

1. INTRODUCTION

Detection and processing of VHF and UHF Satellite cw signals with power levels less than -135 dbm at the antenna present difficulties when attempting to translate the processed data into meaningful measurements of ionospheric physical interactions. The principal problem is interference from extraneous signals, that is, man-made and natural rf noise. For several years tracking filters have been employed to alleviate the problem by narrowing the receiver bandwidth to a few cycles per second. The filters are required to frequency track the rf signal, because generally the satellite signal and the local oscillator are not sufficiently stable to allow use of a narrowband fixed filter.

Experience has shown that geostationary satellite UHF signals drift up to 200 Hz and orbiting satellite signals, due to the added doppler frequencies, shift many times that amount. Local oscillators, however, can be made extremely stable using synthesizer techniques.

The complexity of the tracking filter with the automatic search circuitry required to lock the filter onto the signal during acquisition, or when it reappears after a fade, is an unattractive feature of this process.

(Received for publication 1 June 1976)

Experience has also shown that when the signal is scintillating violently the tracking filter will not stay locked. For these reasons, and the difficult alignment procedure, it appears that frequency tracking is not the solution for low-cost satellite monitoring receivers, although, in most cases, it is the only solution at present.

2. PHASE MEASURING EQUIPMENT

Fortunately there are satellites transmitting high and low UHF signals that are coherent; that is, both are multiples of the same crystal frequency and, as a consequence, lend themselves favorably to a simpler, much more dependable and less expensive system for their detection and processing. This is a cross-correlation technique designed at the AFCRL Ionospheric Research Laboratory, Bedford, MA to measure differential phase between a 40-MHz signal and a 360-MHz signal transmitted from the ATS-6 satellite. If the use of electronic correlation is not restricted because of the required response time, it is a powerful tool capable of extracting minute but meaningful information from an exceptionally noisy environment. The bandwidth determined by the integration time constant can be made extremely narrow. In this system it is 0.5 Hz at -3 dB, this being adequate for the fastest 360° phase shift encountered.

Inspection of the cross-correlation formula, $\phi(\tau) = 1/T \int_0^t f(\tau)\, g(t - \tau)\, dt$ shows that when two time-varying voltages f(t) and g(t - τ) are the same frequency and the delay time τ is zero, the signals will be in phase and the output voltage, $\phi(\tau)$ will be a maximum positive dc voltage. As τ varies, the phase between the voltages increases. At 90° the average correlated output is zero. When τ is such that the phase difference is 180°, the correlated output is a maximum negative dc voltage. If τ is varied linearly in incremental steps, using a tape loop, for instance, to provide g(t - τ), the correlated integrated output is sinusoidal with each incremental step's worth of integrated data being produced for each cycle of the tape loop.

The use of cross-correlation to detect and process ionospheric phase data provides a compatible marriage between the processing technique and the phenomena producing the ionospheric anomalies for the following reasons:

(1) The transmitted frequencies are made coherent in the satellite, therefore, frequency locking equipment is not required for this equipment.

(2) The variable delay (τ) does not require any additional equipment as it is generated naturally in the ionosphere by the diurnal variation of the total electron content, with its inherent refractive effects changing the phase velocity of the 40-MHz signal. τ is also sensitive to phase scintillations and faster changes in

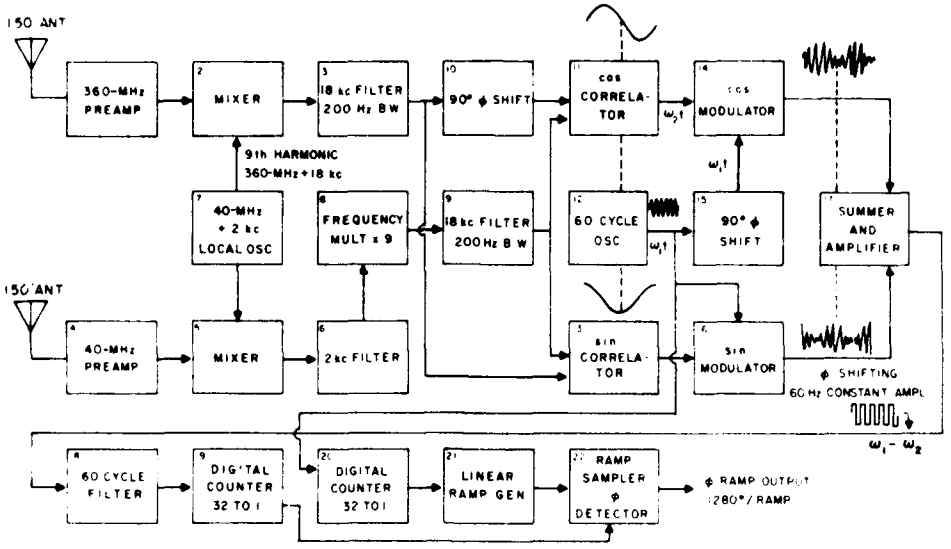

Figure 1. 40- and 360-MHz Differential Phase System Block Diagram

the total electron content (TEC), such as those caused by magnetic storms and ionospheric winds; also traveling ionospheric disturbances, that is, acoustic-gravity waves that modulate the TEC profile as they propagate through the ionosphere.[1]

(3) Because the system rejects random noise and uncorrelated signals, the products of which average out to zero, the normal receiver requirements are minimal, and it is not necessary to employ a complex phase locked communications receiver.

(4) The circuitry that provides a 0.5 Hz bandwidth also produces a quasi-sinusoidal integrated output voltage when the TEC is increasing or decreasing at a linear rate. By coincidence, and very conveniently, this satisfies the first requirement for generating a voltage proportional to phase for making a strip chart recording.

A block diagram (Figure 1) has been provided to assist in the explanation of the complete system. The receiver portion consists of blocks 1 through 7. Blocks 1 and 4 are standard preamps with a 2 dB noise figure and a 28 dB gain. The local oscillator, block 7, is tuned 2 KHz higher than the 40-MHz satellite signal; thus, when mixed with the satellite signal, 2 KHz becomes the difference frequency for further processing.

1. Yeh, K.C. and Liu, C.H. (1974) Acoustic-Gravity waves in the upper atmosphere, Rev. Geophys. Space Phys. 12(No. 2):193.

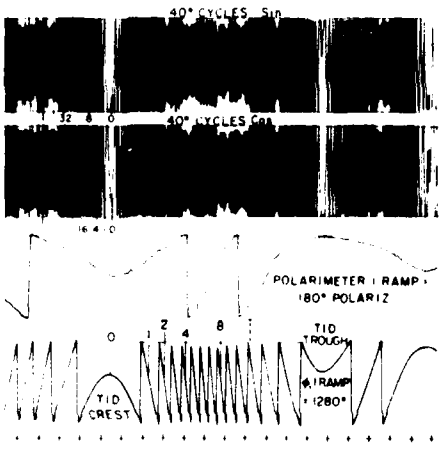

Figure 2. Square Law Spacing of Phase Cycles Indicating a Linear Separation Rate of the 360-MHz and Refracted 40-MHz Rays

When the local oscillator is mixed with the 360-MHz satellite signal it is actually the 9th harmonic that is used, thus making the 2 KHz difference frequency 18 KHz for further processing at the mixer output.

At this point the system has produced a 2-KHz signal carrying the 40-MHz phase information and an 18-KHz signal to be used as the standard, since refractive effects on the 360-MHz frequency responsible for it are minimal.

The two frequencies have remained coherent through the heterodyning process. because the same L.O. has been employed for both; however, for cross-correlation purposes they should both be the same frequency. To accomplish this the 18 KHz could be divided down to 2 KHz or the 2 KHz could be multiplied up to 18 KHz. The latter method was chosen for two reasons. There is more stability in frequency multiplication than there is in frequency division, and it is possible to make a chart record that is nine times more sensitive, nine being the multiplication factor to bring 2 KHz up to 18 KHz. Therefore, each $\phi(\tau)$ cycle out of the correlator represents 40° instead of 360° of the 40-MHz phase change. See Figure 2.

The increased sensitivity is valuable when measuring the time of occurrence of TID's (Figure 2) as the phase reversals can be measured accurately to within a few degrees. Its potential value is the accuracy to be achieved in measuring TID direction and speed, if three systems are put into operation in triangulation.

For strip chart recording of phase and phase scintillation, a sinusoidal function is not adequate as it is subject to ambiguity, that is, one cannot tell if the phase is increasing or decreasing. If the system includes two correlators, one generating a sinusoidal function and the other generating a cos function, as this system does (blocks 10 through 13), the ambiguity can be

eliminated through visual interpretation of the record. However, this is a tedious operation, so it is better to extend the process further and include a coordinate converter (blocks 12, 14, 15, 16, 17) that puts the data back in the form of two coherent ac signals still retaining the proper phase relationship that can operate a phase ramp generator. The frequency can be whatever one chooses. This system uses 60 Hz because of future intentions to drive a clock motor. It may appear at this point that nothing has been gained; we started with two 18-KHz signals, one changing phase relative to the other, and we end up with two 60-Hz signals, one changing phase relative to the other. The big difference, however, is that the unprocessed 18-KHz signals have so much phase jitter and extraneous noise that the data from a phase detector operating on these signals would be worthless. On the other hand, the two 60-Hz signals are relatively noise-free having gone through the correlation process with the 0.5 Hz bandwidth.

Mathematical expressions describing the more complex portions of the system are as follows: Placing a 90° phase shift on one of the 18-KHz signals and simultaneously running it through a second correlator produces a second correlated signal, thus providing two output voltages, $\sin \phi(\tau) = 1/T \int_{\circ}^{t} f(t)\, g(t-\tau)\, dt$ and $\cos \phi(\tau) = 1/T \int_{\circ}^{t} f(t)\, g(t-\tau)\, dt$.

When the phase between the two input signals is shifting at a constant rate, these two functions can be considered to be very low sub audio frequencies, one 90° out of phase with the other. One cycle per second is about the highest frequency encountered so far. Therefore, treating them as such yields the following expressions for the output of the modulators: box 14, $(\sin \omega_1 t)(\sin \omega_2 t)$ and box 16, $(\cos \omega_1 t)(\cos \omega_2 t)$. Summing the two outputs (box 17) yields the trigonometric relation, $\cos(\omega_1 t - \omega_2 t)$. Amplifying this signal into saturation obliterates the cos function and the output is then $t(\omega_1 - \omega_2)$. Thus the output of the summer and amplifier when $\omega_1 = K = 60$ Hz and $\omega_2 = 1$ Hz is a 59-Hz square wave which is just another way of saying a 60-Hz constant amplitude voltage is changing phase at the rate of one cycle per second relative to the 60-Hz standard.

The multiplication by 1/T is performed to normalize the data, that is, to eliminate signal time duration as a factor in determining the amplitude of the integrated output.

Operating a conventional phase detector off of the two 60-Hz signals produces a phase ramp for each 40° phase shift between the two rf signals at the antenna, that is, 360°/9 as explained earlier in the text.

It was decided, however, not to phase detect here, but to extend the range to 1280° per ramp to help distinguish phase scintillations from phase ramps and also to reduce the chart speed for more economical use of chart paper. To accomplish this both 60-Hz signals are fed into 32 to 1 digital counters, (boxes 19, 20). The counter output, operating from the 60-Hz oscillator, supplies a pulse to repeatedly

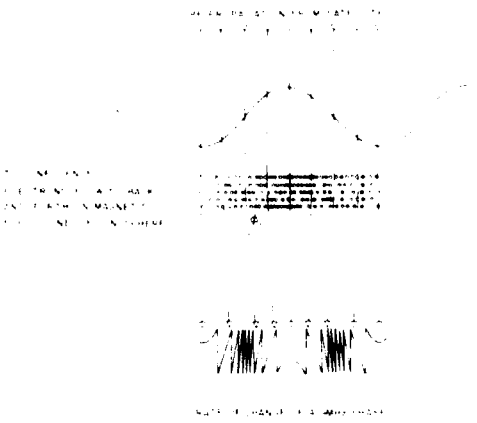

Figure 3. Influence of Traveling Ionospheric Disturbance on Electron Content and RF Propagation Using Geometry at Equator for Simplification

start a very linear ramp generator (block 21). This is a sawtooth voltage with a repetition rate of approximately 0.5 cycles per second, that is, 32/60 Hz.

The ramp generator is fed to the phase detector where it is sampled by the instantaneous pulse from the 32 to 1 signal counter. The value sampled is placed in storage on a capacitor and held constant until the next pulse 2 seconds later. If the phase is increasing, the sampled values follow the ramp up in the positive direction. If the phase is decreasing, the reverse is true. For example, if it takes 32 seconds for the signal to complete each cycle of the 2-second ramp in incremental stored steps, the output of the phase detector is a 32-second ramp that reverses direction when the signal reverses phase. See Figure 2.

Earlier in the text it was mentioned that there was a reason for using 60 Hz in the coordinate converter. The proposal is to develop a complete diurnal curve of the total electron content using electromechanical techniques. If the two 60-Hz voltages (blocks 12 and 17) are used to drive clock motors, the output shaft of the signal 60 Hz will rotate slightly faster or slower than the standard 60-Hz motor, depending on how fast the phase is increasing or decreasing. By using an appropriate gear reduction in combination with a mechanical differential, coupled to a linear potentiometer, it will be possible to develop a variable dc voltage representing a diurnal plot of the electron content, there being a direct correlation between phase shift and changing TEC. The gear reduction will have to be sufficient to keep the rotation of the potentiometer arm within the mechanical limits of the potentiometer. This will ensure a smooth curve without interruption caused by potentiometer discontinuity.

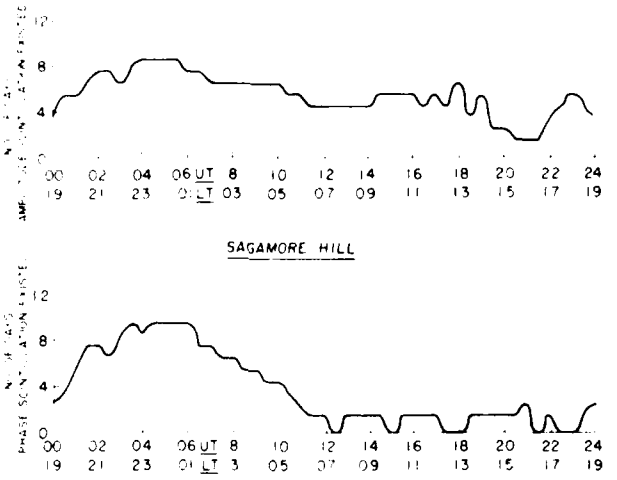

Figure 4. Statistical Comparison of Amplitude and Phase Scintillation

3. COMPARING AMPLITUDE SCINTILLATION WITH PHASE SCINTILLATION

The equivalent thin phase screen" is a popular concept used by ionospheric scientists for explaining, in mathematical terms, amplitude scintillations on rf signals propagated through the ionosphere. This is a screen of negligible thickness that would produce the same phase variations on the rf signal as the actual irregular region.[2] The assumption is that the signal leaves the thin screen, fluctuating in phase only but, as the wave propagates beyond the screen, amplitude fluctuations develop from the summation of the deviated phase signals.

Recent measurements made on ATS-6 geostationary satellite signals comparing 40-MHz phase with amplitude show that application of the equivalent thin screen theory is valid for only a portion of the data. During a 13-day active period of ionospheric scintillation in November 1974, data was computerized to make the above comparisons. The results show that during the periods of amplitude scintillation, phase scintillation existed only 53 percent of the time (Figure 4). Thus, if the amplitude scintillation at the antenna was not the result of ionospheric phase scintillation during 47 percent of the time, another theory is required to explain the results. To conform to the data as presented on the strip charts, the responsible mechanism must allow both enhancement and attenuation of the rf signal. Past investigators studying large-scale irregularities have

2. Briggs, B.H. (1966) Brief review of scintillation studies, Radio Sci. 1(No. 10):1163.

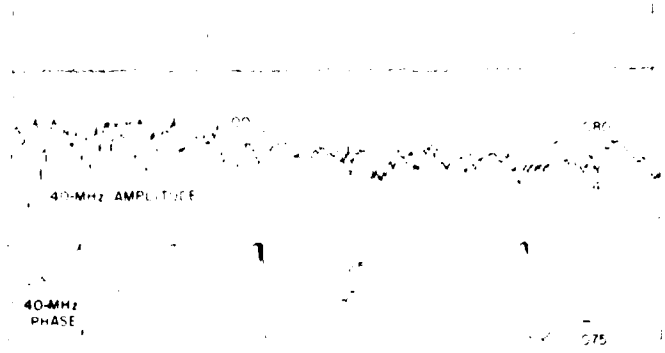

Figure 5. Amplitude and Phase Scintillation Occurring Together

suggested marked focusing effects as the cause of scintillation. This could also explain the remaining 47 percent reported here. Concurrent cycles of the rf propagation could be focused on the antenna through lens-like structures of the irregularities, eliminating the phase deviation requirement dictated by the diffraction theory. Also, when a moving ionospheric structure focuses an increase in energy on the antenna, its refractive area that supplied the enhancement must also reduce the energy when it is appropriately positioned, resulting in moving irregularities that are equivalent to alternating convex and concave lenses.

In a similar manner, moving electron gradients normal to the propagation path could deflect concurrent rays that are close to grazing incidence resulting in alternating enhancement and fading of the signal at the antenna.[3] An example of amplitude scintillation accompanied by phase scintillation is shown in Figure 5; amplitude scintillation without the presence of phase scintillation is shown in Figure 6.

A graph (Figure 7) was constructed showing the percentage of time the phase angle ϕ was in excess of x degrees for the 13-day period. The smoothness of the curve suggests that sufficient data was analyzed to describe conditions for a high percentage of ionospheric scintillation.

Although the shape of the curve appears to indicate a near Gaussian distribution of irregularities with respect to the line of sight between the satellite and the receiver, logically there is no reason to believe there would be such a distribution at the specific region where the rf ray penetrates the ionosphere. It is more likely that, statistically, there is a linear distribution being affected by a diminishing power law.

3. Slack, F. F. (1971) Quasiperiodic scintillation in the ionosphere, J. Atmos. Terr. Phys. 34:927.

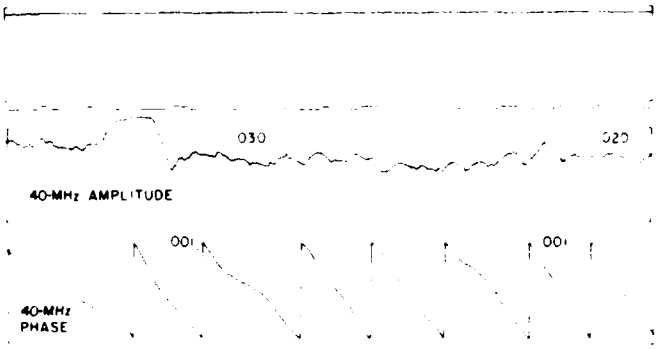

Figure 6. Amplitude Scintillation Without Phase Scintillation

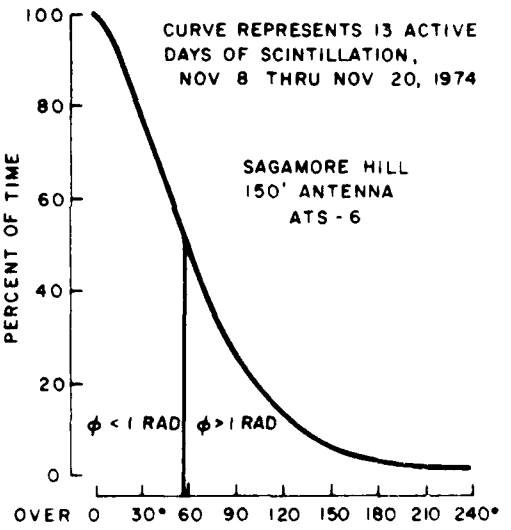

Figure 7. Phase Scintillation in Degrees

The Fresnel formula, $vt = \sqrt{2n\lambda r}$ states that when the lateral distance in the ionosphere between the line of sight ray and an interfering ray, or the equivalent radius resulting from diffracted or scattered rays has changed vt, it produces a difference in the arrival time required for nλ at the receiver distance r. If $\tau_o/2\pi$ is substituted for n, the equation can be solved for phase change τ_o instead of integers of wavelengths. Thus with rearrangement and substitution, the formula becomes

$$\tau_o = \frac{\pi (vt)^2}{\lambda r}. \qquad (1)$$

From this it is apparent that the change in phase resulting from a linear distribution is proportional to the square of the ray separation distance vt. Looking again at the graph in the region of $\tau_o > 1$ rad, the curve closely follows a square law indicating Fresnel action on a linear distribution of irregularity sizes. If such is the case, it supports the contention made by several investigators that some ionospheric scintillation is produced by either a superposition or a distortion of quasi-periodic events. These are the irregularities which, when isolated, develop a characteristic "ringing" Fresnel pattern as displayed on the amplitude channel of a chart recorder.[4, 5, 6] They fall in the region $\tau_o >> 1$ rad, and the curve would have to be extended significantly to include the uncontaminated, isolated examples.

The region of $\tau_o < 1$ rad is where, according to Hewish,[7] and generally accepted by others, the projected irregularities have the same scale size when measured on the ground as would be the case if measured at the ionospheric level. Here the curve is quite linear, as one might expect with a linear distribution of increasing scale sizes, because the change in refractive index, and thus the change in phase, is directly proportional to the electron content in the irregularity. Aarons et al[8] in referring to the two regimes as weak scattering where $\tau_o < 1$ rad and strong scattering where $\tau_o > 1$ rad shows that there are periods when the two regimes exist simultaneously. The graph supports their findings by displaying a gradual transition from linear to a characteristic Fresnel curve in the region between 57° and 90°.

The recorded data does not differentiate between positive and negative phase deviations, so they all have been lumped on one side in the graph. Since τ_o is the result of a changing refractive index about a mean level, a complete graph should include a mirror image of itself in the negative τ direction to more accurately portray the process that produces the phase scintillations. This is taken into consideration in explaining the non-linearity of the curve close to $\tau_o = 0$. It is similar to the zero beat that appears on a traveling ionospheric disturbance

4. Elkins, T.J. and Slack, F.F. (1969) Observations of traveling ionospheric disturbances using stationary satellites, J. Atmos. Terr. Phys. 31:421.
5. Titheridge, J.E. (1971) The diffraction of satellite signals by isolated ionospheric irregularities, J. Atmos. Terr. Phys. 33:47.
6. Kelleher, R.F. and Martin, P. (1975) Fresnel-type fading on satellite records at low latitudes, J. Atmos. Terr. Phys. 37:1109.
7. Hewish, A. (1951) The diffraction of radio waves in passing through a phase-changing ionosphere, Proc. R. Soc. A209:81.
8. Aarons, J., Castelli, J.P., and Kidd, W. (1962) Cygnus rise and set measurements at VHF and UHF radio frequencies, Proc. Internat. Conf. Ionos., 252.

record (Figure 3) when the phase reverses direction, and the angular refraction goes to zero.

In comparing the information contained in Figures 4 and 7, and using a spate of speculation with at least a modicum of logic, it appears that there is a relation between ζ scintillation in the hours between sunset and sunrise and $\phi_o < 1$ rad. Since the electron content is decaying during this period, and the electrons would be clinging to their magnetic field aligned positions, electron gradients would develop normal to the field. With the ionosphere in motion, conditions now exist for the occurrence of ζ scintillations, initially falling in the regime $\phi_o < 1$ rad, because adjacent areas would produce only slight differences in refraction. As the decay cycle continues, electron deficient holes would likely develop because of the remaining electrons' propensity for field alignment, causing the medium to become more irregular. At this time there would be a tendency towards focusing mechanisms or grazing reflection surfaces more suitable for ζ scintillations in the regime $\phi_o > 1$ rad. Briggs[1] in writing about "the equivalent thin phase screen" and its application to scintillation amplitude, summarized by saying, "This method will give useful results if $\phi_o < 1$ rad. When ϕ_o is large there is evidence of focusing." Note in Figure 4 the negative correlation between ζ scintillation and amplitude scintillation during the daylight hours. Then compare this with Figure 7 showing that the rate of occurrence of ζ scintillation is practically zero for $\phi_o > 240°$. Thus the data indicates that during the daylight hours the increased electron density requires that the irregular structure instead of behaving like holes must now behave as cylinders with essentially all amplitude scintillations being caused by focusing or reflection surfaces, that is, ζ scintillation is almost nonexistent, and when it does occur it is likely to be in the regime $\phi_o > 1$ rad.

It must be emphasized that the above explanation has been based on 13 active days of scintillation in November and its application to scintillation in general is a matter of conjecture.

4. THE TRAVELING IONOSPHERIC DISTURBANCE

One of the most outstanding features displayed by the phase data is the influence that traveling ionospheric disturbances (TID) have on the phase of the 40-MHz signal. A TID is generally thought to be an acoustic-gravity wave propagating through the vast expanse of the atmosphere including the ionosphere.[1]

Interpretation of the data (Figure 2) indicates that the medium is being diffused and compressed in a cyclic manner that changes its refractive index in the same fashion. Further, the data shows that the alternating diffusion and compression is in a direction that crosses the satellite receiver propagation path. To

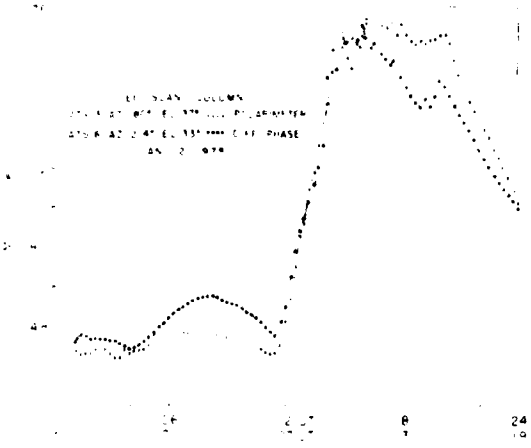

Figure 8. TEC Slant Column

reach this conclusion consider the diurnal curve of the total electron content (Figure 8). This is the sum of all the phase ramps into one continuous 24-hour curve. Since there is a direct correlation between TEC and phase, the ordinate of the curve can be calibrated in the number of electrons per m^2 column between the satellite and the receiver. Polarimeter data has been used this way for a number of years but uses the relationship between TEC and Faraday rotation and is only about 10 percent as sensitive to the changes in the medium. Also the polarimeter measures the Faraday rotation only to the range still influenced by the earth's magnetic field. Because of this difference the electron content, as measured by the polarimeter, should never exceed the differential phase TEC measurements. Since the figure contradicts this fact, it appears that the wrong range value was selected in the polarimeter analysis.

The figure shows that the TID produce equal deviations about the median of the curve. This indicates that there has been no net gain or loss in the total electron content, only that the electrons have been diffused away from the satellite-receiver propagation path and then compressed back again. If the compression and diffusion were in the direction of the rf path, the data would show no change in the total electron content column when TID are present.

Since the ion gyrofrequency is much higher than both the ion neutral collision frequency and the wave frequency, the charged particles can move only along the magnetic field lines.[1] Thus ionospheric oscillations are induced more easily by field aligned perturbations. Combining this information with the above presents the hypothesis that the extent of TID influence on the rf propagation path is latitude dependent, being maximum at the equator where the satellite-ground propagation path is normal to the magnetic field lines, and minimum in the northern latitudes where the ray path and field lines are more closely parallel.

This, of course, excludes other factors that may be more overpowering, such as the TID having spent its energy by the time it reaches the equator.

The ATS-6 satellite elevation angle at Sagamore Hill, Hamilton, Massachusetts is 36°. The magnetic dip angle is 73°. Therefore the rf propagation path crosses the magnetic field lines at an angle of 37°. It follows that the magnitude of the electron flow, normal to the propagation path, is sin 37° x the magnitude of the electron motion moving back and forth along the field lines as they respond to the TID wave motion. This compares with sin 90° at the equator.

It is also important to consider the TID direction component normal to the rf propagation path, so that the refractive process taking place can be understood, since this is what the receiver and phase detector system is measuring. If the crest of the TID wave represents the maximum electron density and the trough the minimum (Figure 2), then one can visualize this as introducing ionospheric gradients in the direction of the TID motion with maxima and minima representing positions where the rate of change of electron content goes to zero. Zero angular refraction (no bending of the rf ray) would appear when these points are centered on the ray; more specifically, when components normal to the ray have reached this condition, that is, the integrated column of electrons are equal on opposite sides of the ray in the incident plane. It follows then that maximum refraction occurs when the rate of change of electrons is greatest during the steepest part of the TID wave. This is just what the recorded data shows, except that these conditions are slightly offset by the ever present diurnal change in total electron content.

The earlier section on the equipment shows how these physical interactions are translated into electrical measurements that are displayed on a chart recorder. A better understanding is provided by studying the diagram (Figure 3). The diagram represents conditions in the ionosphere where the satellite is directly overhead; the magnetic field lines are at right angles to the rf propagation path, and the TID direction is also normal to the rf propagation path. The figure shows what happens to the rf ray as a TID influenced electron gradient moves across it. No bending occurs at the maximum and minimum positions where there is zero gradient. Maximum bending occurs during the steepest portion of the gradient. Since the refractive index is less than one, the bending is always towards the greater density.

As the gradient passes across the ray, the phase velocity completes a cycle of increasing, decreasing, and reversing direction, then increasing and decreasing in the reverse direction. One side is a mirror image of the other except for the imbalance caused by the diurnal effect, or some other natural perturbation. This action repeats for each passing TID cycle that intercepts the rf ray and is illustrated on the strip chart (Figure 2).

There have been pen recordings showing examples of TID electron displacements up to 20 percent of the ambient total electron content at the time of the disturbance. Close inspection of the phase data 40° cycles and 1280° phase ramps shows that the refraction generally is causing the 40- and 360-MHz rays to separate and close at a constant velocity, which, in turn, causes typical doppler spacing of the 40° cycles. The cycles follow the square law spacing for a constant velocity fixed frequency moving at right angles to the propagation path. A mathematical solution shows that doubling the lateral distance the ray travels produces four times the number of cycles. Note, on Figure 2, that doubling the 2-cycle distance produces 8 cycles, and doubling the 4-cycle distance produces 16 cycles. It is assumed that the dominant action is on the 40-MHz ray, the coherent 360-MHz being high enough to be almost free of the refractive effects and is thus used as the standard reference for the phase measurement.

It should be emphasized that the number of cycles between crest and trough per unit time does not measure the velocity of the TID, but relates to the rate of separation and closing of the 40- and 360-MHz rays normal to the propagation path. The number of cycles are also a measure of the TID amplitude; that is, the bigger the TID, the greater the influence on the electron density which, in turn, produces a larger change in refractive index and, thus, an increase in phase velocity, as illustrated on the chart, by recording a greater number of cycles per unit time.

Doppler theory adequately explains the form of the data as displayed on the chart record; however, many of the parameters that influence space communications can be gleaned from the data through the application of ray optics analysis, which then permits the use of Snell's law and the Appleton Hartree formula. A list of these parameters in addition to total electron content (TEC) are:

(1) Changes in electron density, assuming height
(2) Slab thickness, assuming height
(3) A continuous measurement of phase velocity
(4) A continuous measurement of rate of change of TEC
(5) A continuous measurement of refractive index
(6) A continuous measurement of angle of arrival

A simple analysis can be performed on the recorded data, on those sections where the chart record clearly indicates that the phase is shifting in accordance with a linear motion normal to the rays; that is, the 40° cycles follow the square law spacing mentioned earlier. There are, generally, several such sections to be found each day.

Ray optics analysis is valid if the following conditions are met: (1) the incident angle ϕ_i is sufficiently large; (2) the medium is lossless; (3) the phase is

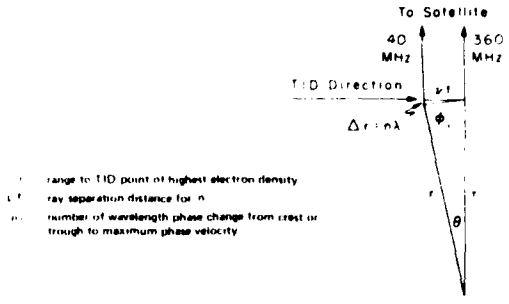

Figure 9. The Geometry for the Case Where the Satellite Is Directly Overhead and the TID Direction Is Normal to the rf Ray

measured at a distance sufficiently far from the inhomogeneous medium; and (4) the media vary slowly compared to a wavelength.[9] These conditions exist for the data presented. The first condition exists because gradients normal to the ray path caused by the TID are considered to be the dominant influence on the rf ray; therefore, the incident angle τ_i is measured from a line normal to the gradient. Figure 3 shows that τ_i is always very large going to 90° at both the crest and trough of the TID. Since total reflection occurs in all dielectrics at the grazing incident angle (90°), the principle of reversibility[10] can be used to explain the phase reversal at both the crest and trough. The principle of reversibility states that whenever a ray is totally reflected a phase change of 180° occurs; also, if the phase reversal does not take place when the wave passes from the lower to the higher refractive index, it will occur when the wave passes from the higher to the lower refractive index. This explains, through ray optics, the phase reversals appearing on the chart records at both the TID crest and trough. Thus, ray optics theory provides the same answer given by the phase doppler process which shows the frequency or phase to be increasing when range of the rf source is decreasing, and decreasing when the range is increasing, with a phase reversal at or near the point of closest approach. Figure 9 depicts the geometry for the case where the satellite is directly overhead and the TID direction is normal to the rf ray.

9. Papa, R.J., private communication.

10. Jenkins, F.A. and White, H.E. (1937) Fundamentals of Optics, McGraw-Hill, New York.

Solving the geometry yields some important relationships:

$$r = \frac{(\nu t)^2}{2n\lambda} \quad \text{and}$$

$$\nu t = \sqrt{2n\lambda r}. \tag{2}$$

This is recognized as the Fresnel formula when $n = 1$, and states that the ray separation or closing must have traveled νt in order to change the phase 360° at the distance r.

If the incident angle ϕ_i is measured from the path νt, a line normal to the TID gradient, the relationship $\nu t / r = \cos \phi_i$ is important, because it accommodates the introduction of an equation derived from Snell's law, $\cos \phi_i = f_N / f$ where f_N = plasma frequency and f = the propagation frequency. From the Appleton-Hartree equation: $\mu^2 = 1 - \chi = 1 - (f_N/f)^2 = 1 - KN/f^2$, where μ = the refractive index, $K = (e^2/4\pi^2 \epsilon_o m) = 80.6$, f is in Hz, N = number of electrons/m^3 at highest density point. Combining these equations gives:

$$f_N = \sqrt{80.6N}$$

$$\cos \phi_1 = \frac{\sqrt{80.6N}}{f} = \frac{\nu t}{r} = \frac{2n\lambda}{\nu t} = \sin \theta$$

$$r = \frac{2n\lambda f^2}{80.6N} \quad \text{or} \quad N = \frac{n\lambda f^2}{40.3r}. \tag{3}$$

The last expression states that if the range to the point of highest electron density is known, the change in density caused by the TID can be calculated. However, it must be remembered that the equation represents conditions when the 40- and 360-MHz rays are separating at a linear rate, and it is only during the periods when the chart records show this that the analysis can be performed.

To ascertain the TID velocity, three spaced differential phase sites could be established. The TID velocity would be calculated by making appropriate use of the time difference of the phase reversals at the three sites. As stated earlier, these are the times when the angular refraction has been reduced to zero, thus the measurements provide accurate information regarding the TID crest or trough position, speed and direction.

Range (r) to the area of maximum density can be measured, if phase data as a function of relative TID position among the three sites is separated from phase data caused by ionospheric refraction. This can be accomplished using

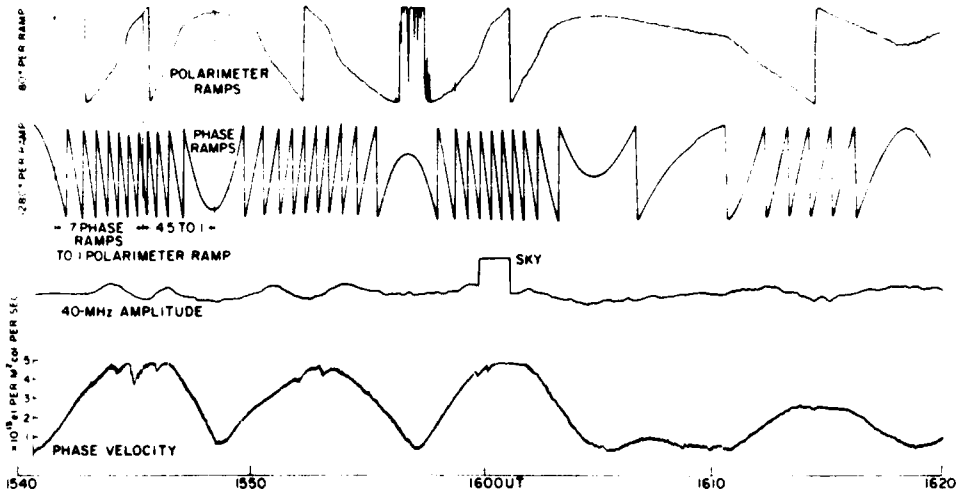

Figure 10. Changing Phase and Polarimeter Ramp Ratio Caused by Series of TID

interferometer analysis on the higher frequency (360-MHz) by knowing the various distances among the three sites. However this is the subject for a later report, should the expanded program materialize.

Analysis of the data shows the tremendous influence a TID has over the ionospheric refraction of the lower UHF signals. In minutes it can reduce to zero the rate of change of electron content and temporarily reverse the diurnal refractive process caused by the sun. The reason for this is the dominance of the TID gradients normal to the ray path giving rise to large incident angle (including grazing), as opposed to the normal, less disturbed vertical gradients with incident angles that are much more acute. This is in accordance with Snell's law; the more oblique the angle, the lower the plasma frequency, resulting in greater refraction.

If one accepts the foregoing analysis, one must ask the question, "How can the ramps measure the electron density per m^3 and, at the same time, measure the electron content in a square meter column between the earth and the satellite?" The answer is that during TID they cannot, because the formula for electron content is invalid where horizontal gradients are present. This is demonstrated in the following exercise.

Shortly before the ATS-6 satellite disappeared over the horizon, a 40-MHz polarimeter output was fed on to an adjacent pen recorder channel for comparison with the differential phase data (Figure 10). During this nine-day period

there were some interesting revelations. The ratio of polarimeter ramps to differential phase ramps varied during the day. Since both were presumed to be a measure of the electron content in a square meter column between the satellite and the receiver on the ground, except for a small difference caused by the plasmasphere, it was expected that this ratio would be nearly constant. This proved to be a false assumption. The two measured extremes are 7 to 1 and 4 to 1. Shown in the figure is a ratio of 4.5 $\Delta\phi$ ramps to 1 polarimeter ramp and a ratio of 7 to 1 at an earlier time.

In terms of electron content, the formula for the differential phase is:

$$\Delta\phi = \frac{1.34 \times 10^{-7}}{40\ \text{MHz}} \left(\frac{m^2 - 1}{m^2}\right) \text{TEC}$$

where $\Delta\phi$ = number of 360° phase shifted cycles between the low frequency and the high frequency and m = 360-MHz/40-MHz. The ramps displayed on the chart record have been divided down and represent 1280° of differential phase, making one ramp equal to 1.07×10^{15} e/m^2 column.

The formula for converting the polarimeter measurements to electron content is $N_e = \theta/(K/f^2)$ H cos θ and one ramp equals 3.7×10^{15} e/m^2 column. The difference between the two measurements is important. The differential phase system measures the electron content in the total path (the ionosphere plus the plasmasphere) whereas the polarimeter data is a measure of the electron content only to the range still influenced by the earth's magnetic field. Thus, where the ramp ratio is 4 to 1, the change in electron content measures 4.28×10^{15} e/m^2 column in the differential phase system for each 3.7×10^{15} e/m^2 column change in the polarimeter system. This leaves a change of $.58 \times 10^{15}$ e/m^2 in the m^2 column between the magnetic field and the satellite, which seems to be high but perhaps reasonable. However, when the ratio becomes 7 to 1, it represents, in terms of electron content, 7.4×10^{15} e/m^2 to 3.7×10^{15} e/m^2 which states that one half of the electron change in the m^2 column is in space beyond the influence of the magnetic field. This is unrealistic and requires another explanation for the inconsistency in the ramp ratio.

The reason for the inconsistency became apparent when the TID records were given closer inspection. Figure 11 is a 2-hour graph of the differential phase, polarimeter ramp ratio vs. time. Each low point corresponds with the point of zero angular refraction where the phase reverses direction and the electron diffusion is greatest (Figure 10). The high points coincide with periods of highest phase velocity (maximum angular refraction). This gives convincing evidence that the presence of the TID is responsible for the changing ratio. It is inconceivable to think that the TID could double the influence of the magnetic field,

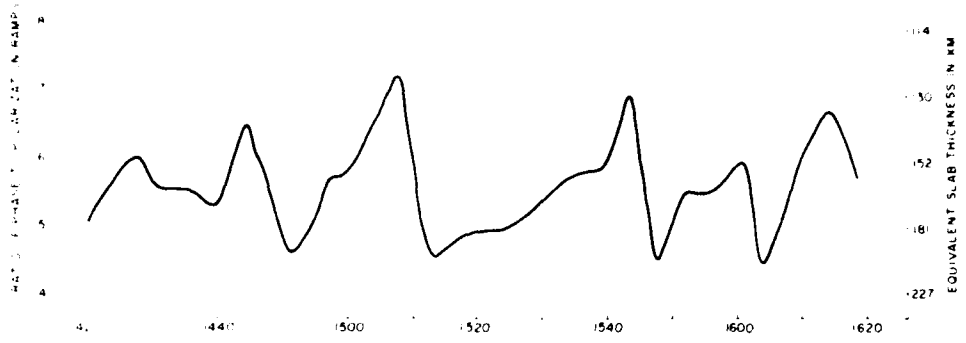

Figure 11. Changing Phase and Polarimeter Ramp Ratio Caused by TID, Also Showing influence on Slab Thickness

and unlikely that the TID would encounter sufficient plasmasphere electrons to produce twice the refraction. Therefore, the conclusion drawn from the above exercise is that the differential phase formula for calculating electron content is not valid in the presence of TID, because it produces horizontal gradients that dominate the physical interactions; thus, the angular refraction is better represented by the derived formula for electron density.

5. ADDITIONAL CAUSES OF DISCREPANCIES IN THE FARADAY/$\Delta\phi$ RATIOS

Smith[11] has noted a diurnal variation in the ratio of Faraday rotation Ω to electron content I of up to 30 percent at Puerto Rico. Kersley and Sawbrook[12] report similar discrepancies in Great Britain. Davies et al[13] are in close agreement with ATS-6 phase modulation and Faraday measurements at Boulder showing a 35 percent diurnal discrepancy. They suggest that the changing Ω/I ratio may be due to the diurnal variation in the effective height of the ionosphere, the 35 percent representing a change from 580 km to 1200 km.

The Hamilton, Massachusetts records were inspected for a changing diurnal Ω/I ratio, but none was found in the six available June records. However, it is apparent in the January 12 TEC profile comparisons (Figure 8) that in the early

11. Smith, D.H. (1970) Diurnal variation of the mean Faraday factor at Areceibo, J. Geophys. Res. 75:823.

12. Kersley, L. and Sawbrook, D.J. (1971) Diurnal changes of the mean Faraday M-factor. Joint Satellite Studies Group Report 4:57. Instituto di Onide Elettromagnetiche, Florence, Italy.

13. Davies, K., Fritz, R.B., Grubb, R.N., and Jones, J.E. (1975) Some early results from the ATS-5 Radio Beacon Experiment, Radio Sci. 10(No. 9, 10):785.

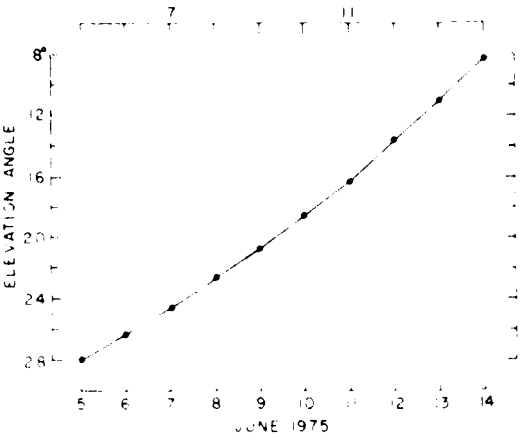

Figure 12. Changing Elevation Angle as ATS-6 Moved Towards Horizon Measured on 150-Foot Antenna

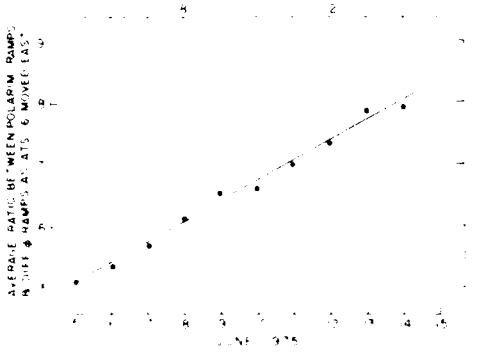

Figure 13. This Changing Ratio Conforms With Theory $\Omega = (K/f^2) \int Ne\, H \cos\theta\, ds$ Where Ω = Number of Polarimeter Ramps, H = Magnetic Field, θ = Angle Between H and Ray Path. θ Was Increasing, Thus cos θ Was Decreasing. The Number of Differential Phase Ramps Is Independent of the Magnetic Field

morning hours from 0000 to 0500 LT the phase is increasing and decreasing much faster than the Faraday rotation, showing values that indicate about 30 percent of the electron content is in the plasmasphere at that time. This would certainly show a much lower Ω/I ratio and indicates a greater effective height during this period, agreeing with the reports by Davies et al.[13]

All other varying Ω/I ratios were scattered through the records and were present as reported above only during periods of apparent horizontal gradients, except for a long-term, changing, average ratio caused by the lowering of the elevation angle as the ATS-6 satellite moved towards the horizon (Figures 12 and 13). Inspection of the TEC equations for both systems shows that the changing ratio conforms with theory, demonstrating that only the number of polarimeter ramps is related to the magnetic field or more precisely to the cos of the angle

between the magnetic field and the ray path. This exercise also serves to demonstrate the validity of the overall equipment design and the field measurements.

6. EQUIVALENT SLAB THICKNESS

Since the form of the phase data during TID is consistent with the formula developed for calculating electron density, calculation of equivalent slab thickness is also possible if polarimeter data is available to measure electron content.

Dividing the electron content contained in the TID wave from the trough to the crest (as measured by the polarimeter), by the electron density for the same period (measured by the Δf method), yields the slab thickness. The ratio, using the parameters given earlier, reduces to:

$$\frac{\text{(no. of 180° polarimeter ramps)}}{\text{(no. of 1280° differential phase ramps)}} \times \frac{(3.5\ h)}{(\sec z)},$$

where h is the height and z is the zenith angle. It is suggested that this ratio is the same as the ratio of TEC to maximum electron density at the time of the measurement. This formula can be used to assign values to Figure 11, which now becomes a very graphic portrayal of the slab thickness profile showing the tremendous influence a TID has on the ionosphere. Using 400 km for h and 1.54 for sec z, it gives values of slab thickness of 126 km to 202 km. These values are practically the same as the ranges reported by Tyagi and Samayajulu[14] using the ratio TEC/max electron density. They reported a range of values from 125 to 200 km at Delhi. However, values reported by Klobuchar and Allen,[15] with combined data from two locations, are higher. Their analysis on data taken for 18 months in 1967-1968 yield a wide range of values with an annual mean value of 261 km. They do caution that the values suffer somewhat from the fact that the TEC data were taken along the oblique path to the ATS-3 satellite from Hamilton, Massachusetts, while the N_{max} values were derived from vertical incidence ionosondes from Fort Belvoir, Virginia and Wallops Island, Virginia.

It appears that more comparison data will be required to determine the validity of the hypothesis that the change in the TID electron content, divided by the change in density, is equivalent to TEC/N_{max}. The following exercise suggests that theoretically they are the same.

14. Tyagi, T.R. and Samayajulu, Y.V. (1966) Some results of electron content measurements from Faraday fading of S-66 transmissions, Radio Sci, 1:1125.

15. Klobuchar, J.A. and Allen, R.S. (1970) A first-order prediction model of total electron content group path delay for a midlatitude ionosphere, AFCRL Report 70-0403, Air Force Surveys in Geophysics No. 222.

The Klobuchar and Allen analysis[15] showed that the propagation delay $\Delta r = 40.3/f^2 \int Ndl$ where $\int Ndl$ = TEC in el/m^2 slant column.

Referring back to the formula for electron density derived here for the TID, it is shown that $N = n^2 f^2/40.3r$ where N = electron density = el/m^3; $n^2 = \Delta r$, thus $\Delta r = 40.3rN/f^2$.

Since there is only one Δr representing the delay in propagation from crest to trough in the TID, irrespective of the cause, the two formulas for Δr can be equated, which yields $r = \int Ndl/N/m^3$. Thus it is shown that such a relationship produces the formula for the equivalent slab thickness; however, in this case the integration is only during the TID interval from crest to trough, and N represents the change in electron density for the same period. This is the equivalent m^2 column of length r, with a uniform density of electrons, that is either compressed into or diffused away from the equivalent m^2 column representing the total electron content with a uniform maximum density. The question is, "Are they really the same length?" The analysis shows that at least they are in the same ball park.

7. ELECTRON CONTENT IN THE PLASMASPHERE

Comparing Figure 10 with Figure 11 shows that the low points coincide with times of maximum diffusion and zero angular refraction. The indication is that all gradients normal to the rf ray have momentarily disappeared, so these are the periods when the differential phase formula for TEC is valid. Thus, if comparisons are made between the TEC diurnal profiles of both systems to measure the electron content in the space between the ionosphere, influenced by the earth's magnetic field and the satellite, the TID troughs would be accurate positions from which to make such measurements. As illustrated in the figure, the trough positions produce the more stable and consistent values, indicating that the averaged net TEC beyond the magnetic field remains quite constant, even though ionospheric perturbations are present during this period.

8. A SUNRISE PHENOMENON

Davies et al[13], using Faraday and modulation phase data from an ATS-6 experiment, have illustrated an interesting sunrise phenomenon. They have shown that the start of the Faraday TEC increase precedes the start of the modulation phase TEC increase, varying from less than 1 minute to 15 minutes

at sunrise. The modulation phase measurement, like the differential phase measurement reported here, measures the TEC all the way to the satellite.

The time difference was attributed to a lowering of the effective height of the ionosphere before the total content starts to increase.

Our records were inspected for this sunrise phenomenon. There were six available records with simultaneous recordings of both phase and Faraday. The delays varied from a few seconds to two minutes.

Comparison of the ATS-6 differential phase profile with the ATS-3 Faraday profile for January 12, 1975 (Figure 10) shows that a large portion of the electron content was in the plasmasphere for several hours before sunrise, reaching a peak of approximately 36 percent of the total at 0315 LT. The data also indicates a fairly sharp demarcation between the ionosphere and the plasmasphere during this period. It is reasonable to believe that the excess electrons were still flowing into the F region at sunrise, thereby lowering the effective height of the ionosphere before new production had actually started, as suggested by Davies et al.[13]

In both the modulation phase measurements and the differential phase measurements, $dI/dt = 0$ occurs when the production rate Q equals the loss rate L. At Boulder, an example was given showing L to be -2.16×10^{12} $m^{-2}sec^{-1}$ at the Faraday morning reversal. In accordance with the above statement at $dI/dt = 0$, $Q = 2.16 \times 10^{12}$ $m^{-2}sec^{-1}$ just after sunrise.

Two Hamilton, Massachusetts records were analyzed for the electron production rate. The analysis yielded values of $Q = 2.19$ and $Q = 2.21 \times 10^{12}$ $m^{-2}sec^{-1}$, agreeing favorably with the Boulder, Colorado measurement.

9. PHASE VELOCITY

The lower channel in Figure 10 is the analog output of a circuit counting the number of 40° cycles per sec. Therefore, it is a measure of the phase velocity. Note that if every other peak is inverted, the trace approximates a slow sine wave 90° out of phase with the trace of the differential phase data, showing it to be the first derivative of the phase analog (the summation of the phase ramps). When it was first recorded, it was calibrated to read the rate of change of electron content per m^2 column between the earth and satellite. However, in view of the new interpretation of the phase data during the periods of TID gradients, it is more accurate to calibrate the data to read rate of change of electron density (electrons per m^3) at highest density region.

References

1. Yeh, K.C. and Liu, C.H. (1974) Acoustic-Gravity waves in the upper atmosphere, Rev. Geophys. Space Phys. 12(No. 2):193.
2. Briggs, B.H. (1966) Brief review of scintillation studies, Radio Sci. 1(No. 10):1163.
3. Slack, F.F. (1971) Quasiperiodic scintillation in the ionosphere, J. Atmos. Terr. Phys. 34:927.
4. Elkins, T.J. and Slack, F.F. (1969) Observations of traveling ionospheric disturbances using stationary satellites, J. Atmos. Terr. Phys. 31:421.
5. Titheridge, J.E. (1971) The diffraction of satellite signals by isolated ionospheric irregularities, J. Atmos. Terr. Phys. 33:47.
6. Kelleher, R.F. and Martin, P. (1975) Fresnel-type fading on satellite records at low latitudes, J. Atmos. Terr. Phys. 37:1109.
7. Hewish, A. (1951) The diffraction of radio waves in passing through a phase-changing ionosphere, Proc. R. Soc. A209:81.
8. Aarons, J., Castelli, J.P., and Kidd, W. (1962) Cygnus rise and set measurements at VHF and UHF radio frequencies, Proc. Internat. Conf. Ionos., 252.
9. Papa, R.F., private communication.
10. Jenkins, F.A. and White, H.E. (1937) Fundamentals of Optics, McGraw-Hill, New York.
11. Smith, D.H. (1970) Diurnal variation of the mean Faraday factor at Areceibo, J. Geophys. Res. 75:823.
12. Kersley, L. and Sawbrook, D.J. (1971), Diurnal changes of the mean Faraday M-factor. Joint Satellite Studies Group Report 4:57. Instituto di Onide Elettromagnetiche, Florence, Italy.

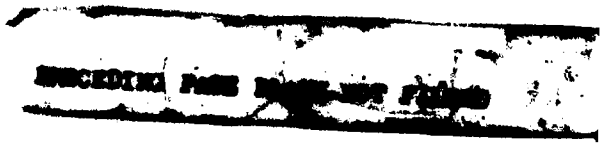

13. Davies, K., Fritz, R.B., Grubb, R.N., and Jones, J.E. (1975) Some early results from the ATS-6 Radio Beacon Experiment, Radio Sci. 10(No. 9, 10):785.

14. Tyagi, T.R. and Samayajulu, Y.V. (1966) Some results of electron content measurements from Faraday fading of S-66 transmissions, Radio Sci. 1:1125.

15. Klobuchar, J.A. and Allen, R.S. (1970) A first-order prediction model of total electron content group path delay for a midlatitude ionosphere, AFCRL report 70-0403, Air Force Surveys in Geophysics, No. 222.